Construction and Building Materials 113 (2016) 783–793

Contents lists available at ScienceDirect

Construction and Building Materials

journal homepage: www.elsevier.com/locate/conbuildmat

Temperature and activator effect on early-age reaction kinetics of alkali-activated slag binders

Berhan Seium Gebregziabiher, Robert J. Thomas, Sulapha Peethamparan *

Department of Civil and Environmental Engineering, Clarkson University, Potsdam, NY 13699, USA

HIGHLIGHTS

- The effects of activators and temperature on activation kinetics are investigated.
- Elevated temperature and increased activator alkalinity greatly accelerate hydration.
- Increased silica retards hydration but improves later-age strength.
- The main product is C-S-H with varying levels of hydrotalcite.

ARTICLE INFO

Article history:
Received 28 June 2015
Received in revised form 3 March 2016
Accepted 19 March 2016

Keywords:
Alkali activation
Ground granulated blast-furnace slag
Reaction kinetics
In-situ calorimetry

ABSTRACT

The early-age reaction kinetics of alkali-activated ground granulated blast-furnace slag (GGBFS) binders as determined by in-situ isothermal calorimetry are discussed in this paper. Particular attention is paid to the effects of activator type (sodium hydroxide and sodium silicate) and concentration, as well as curing temperature (23 °C and 50 °C). The mechanical strength development, microstructure, and product phase composition are also discussed to provide context for the phenomena observed in the kinetics results. It is shown for both activators that elevated temperature curing greatly accelerates hydration, resulting in more rapid product formation and strength development. High-molarity sodium hydroxide activators are shown to accelerate early hydration at ambient temperature, but tend to present a barrier to advanced hydration thereby limiting the later-age strength. Elevated temperature curing is shown to remove this barrier to advanced hydration by improving solubility and diffusivity. Hydration of sodium silicate-activated slag is comparatively slow, resulting in the delayed formation of very dense products with higher mechanical strength. Increasing sodium oxide tends to accelerate hydration, resulting in improved early- and later-age strength, while increasing the silica tends to retard the reaction, resulting in slower, more complete hydration as well as improved mechanical strength.

1. Introduction

Alkali-activated industrial byproducts, and in particular ground granulated blast-furnace slag (GGBFS, hereafter *slag*), have received much attention in recent literature as potential sustainable alternatives to portland cement binders for concrete. The production of portland cement is one of the world's leading sources of carbon dioxide emissions and is a major barrier to the production of sustainable concrete mixtures. The partial replacement of portland cement with beneficiated industrial byproducts like fly ashes and slag has long been employed with noteworthy improvements to the rheology, strength, durability, and heat of hydration [1–7]. Despite its benefits when used in conjunction with portland cement, slag shows only latent hydraulic properties when used as the sole binder. While successful replacements of up to 70% of portland cement with slag have been routinely demonstrated, replacement is often limited to about 40% in North America [7].

In pure water, slag rapidly develops a glassy shell on the grain surface, acting as a barrier to advanced hydration. When used in conjunction with portland cement, the high alkalinity of the pore solution breaks down this barrier, promoting further hydration. When slag is used as the sole binder, an alkaline activating agent like sodium hydroxide or sodium silicate is necessary to promote advanced hydration [8–11]. The resulting binders are predominately composed of sodium and calcium aluminosilicate hydrates (C-A-S-H and N-A-S-H), as well as some hydrotalcite-like products [12–15]. A cornucopia of studies in the past decades have shown alkali-activated slag binders and concretes to be strong, durable,

* Corresponding author.
E-mail addresses: gebregbs@clarkson.edu (B.S. Gebregziabiher), thomasrj@clarkson.edu (R.J. Thomas), speetham@clarkson.edu (S. Peethamparan).

http://dx.doi.org/10.1016/j.conbuildmat.2016.03.098
0950-0618/

and environmentally-friendly, with 10–50% lower associated CO_2 emissions than comparable portland cement formulations [16,17].

The behavior of alkali-activated aluminosilicates is highly dependent on the type and concentration of the alkaline activator and on the curing temperature [18–21]. Elevated-temperature curing greatly accelerates the formation of the microstructure and the development of mechanical strength [22–26]. Sodium silicate-activated slag systems tend to gain strength much more slowly than sodium hydroxide-activated slag, but with significant improvements in later-age strength [13,15,21,27,28]. Increased mechanical strength is attributed to increased silica or sodium oxide in sodium silicate-activated slag. Meanwhile, sodium hydroxide-activated slag sets and gains strength very rapidly [12,20]. This early product formation, however, is accompanied by the formation of a dense reaction ring surrounding incompletely-reacted slag grains and limiting continued diffusion and product formation [15,28]. As such, increased concentration of the sodium hydroxide activator often does not improve mechanical strength.

Several studies have reported in detail on the composition of the hydration products in alkali-activated slag cured at both ambient and elevated temperatures. These studies have concluded that the product phases are generally C-S-H, C-A-S-H, and N-A-S-H, the crystallinity of which increases with age [13,29–31]. Several of these studies have suggested that the composition of the product phases is similar at both ambient and elevated curing temperatures [29,30].

A few early kinetics studies compared the hydration of sodium silicate-activated slag with that of portland cement, concluding that both systems underwent the same basic stages of hydration, viz. wetting, induction, acceleration, deceleration, and steady-state, but that the mechanisms of hydration during these stages were distinct [32–34]. The wetting period in sodium-silicate activated slag is marked by the rapid early formation of C-A-S-H and N-A-S-H gels, and the acceleration period is marked by the later diffusion-limited reaction of larger slag grains [32,34]. Krizan and Zivanovic [35] showed the effect of silica on the kinetics of sodium silicate-activated slag, citing an increase in both the magnitude of the initial heat evolution peak and in the duration of the acceleration period. In addition, Haha et al. [36] discussed the effect of activator type on the hydration kinetics of activated slag, concluding that the high initial rate of reaction in sodium hydroxide-activated slag limited the later-age decrease in coarse porosity, and therefore limited the later-age strength as compared to sodium silicate-activated slag. Much more recently, Gebregziabiher et al. [28] discussed the specific effects of the molarity of sodium hydroxide activators and the silica modulus (relative concentration of silica to sodium oxide) of sodium silicate activators on the hydration kinetics of alkali-activated slag binders cured at ambient temperature. That study showed spontaneous hydration in sodium hydroxide-activated slag, with significant product formation and microstructural development within the first few hours. Increased activator molarity showed a pronounced accelerating effect on the reaction, but did not significantly alter the later-age strength or microstructure [28,36]. Sodium silicate-activated slag, on the other hand, reacted in a slower and more controlled manner. Silica was shown to have a retarding effect on the reaction, allowing for the formation of denser products with higher later-age strength [28]. These observations were consistent with those of Krizan and Zivanovic [35].

Despite the availability of several studies on the reaction kinetics of alkali-activated slag, several important questions remain unanswered. First, it has been well established that curing at elevated temperatures results in much more rapid strength and microstructural development in alkali-activated binders. However, these effect have not been quantitatively evaluated by means of kinetic studies. Additionally, while the effects of activator type and concentration on the hydration kinetics have been discussed to some extent, these discussions have neglected the effect of sodium oxide concentration of sodium silicate activators, focusing instead on the effect of silica in those systems. The present study seeks to address these gaps in knowledge in order to further the understanding of how the activator and temperature affects the rate and degree of hydration in alkali-activated slag binders.

2. Material and methods

2.1. Materials

The raw binder is an ASTM C 989-compliant grade-100 ground granulated blast-furnace slag (slag) sourced from a reputable commercial supplier. The oxide composition as determined by X-ray fluorescent spectroscopy (XRF) is 39.8% CaO, 36% SiO_2, 10.5% Al_2O_3, 7.93% MgO, 2.11% SO_3, and less than 1% of Fe_2O_3, Na_2O, and K_2O. The Blaine surface area is 340 m^2/kg and the loss on ignition is 3%. The particle size distribution as determined by laser diffraction particle size analysis indicates a median particle size of 7.5 μm, with 80% of particle smaller than 10 μm. The X-ray diffraction analysis of the unreacted binder shows a diffuse diffraction pattern typical of an amorphous glassy material.

The alkaline activating agents are aqueous solutions of sodium hydroxide (NaOH) and sodium silicate (SS) ($Na_2O + m{\cdot}SiO_2$, where m is the silica modulus). The former are prepared by dissolving reagent-grade sodium hydroxide pellets in deionized water and allowing sufficient time for heat dissipation. The latter are prepared by diluting a pre-mixed reagent-grade sodium metasilicate solution ($m = 2.5$) with deionized water. The silica modulus m is altered using additions of sodium hydroxide, forming what is actually a compound solution of sodium hydroxide and sodium silicate. The sodium oxide equivalent is determined according to stoichiometry. The mixture details are presented in Table 1. The mass ratio of solution to binder (s/b) is 0.40 throughout.

2.2. Experimental methods

The methods and procedures related to this work are described exhaustively by Deir et al. [15,28] and Gebregziabiher et al. [28]; they are discussed only briefly here. Paste mixtures were mixed in a standard laboratory mixer in accordance with the specifications of ASTM C305. Fresh pastes were cast into the appropriate molds, consolidated on a vibrating table, sealed in plastic, and placed in the specified curing environment. Specimens were either cylindrical, measuring 25 mm in diameter and 50 mm in length, or cubic, measuring 50 mm in each dimension. Cylindrical specimens were used for SEM analyses, and cubic specimens were used for strength evaluation. Specimens were either moist-cured at ambient temperature or heat-cured at elevated temperature. The former was at 23 ± 2 °C and in excess of 95% RH and the latter at 50 ± 0.1 °C. Moist-cured specimens were demolded after 24 h when possible; a few slowly-setting mixtures were demolded after 72 h. Heat-cured specimens remained sealed within the molds to prevent moisture loss during curing.

Compressive strength of paste cubes was determined in accordance with the specifications of ASTM C109 after demolding and 7, 14, 28, and 56 d curing for moist-cured specimens and after 24, 48 and 72 h curing for heat-cured specimens. Microstructural features were observed by backscattered scanning electron microscopy of epoxy-impregnated, polished, and sputter-coated segments sawn from cured cylindrical paste specimens. Specimens were sputter-coated with gold and palladium. Carbon tape was used to maintain conductivity through the sample holder. The elemental composition of the pastes was determined by electron dispersive X-ray spectroscopy (EDS) in conjunction with electron microscopy. More

Table 1
Activator compositions.

ID	Molarity (M)	
Sodium hydroxide		
5 M	5	
8 M	8	
12 M	12	
ID	m	%Na_2O
Sodium silicate		
S1	1.5	2.5
S2	1.5	5.0
S3	1.5	7.0
S4	2.5	2.5

than one dozen representative points per sample were used for EDS analysis. The experimental parameters have been describe in great detail by Deir et al. [15] and Gebregziabiher et al. [28].

Reaction kinetics were studied using in-situ isothermal conduction calorimetry in accordance with the specifications of ASTM C1702 at 25 °C and 50 °C. Calorimetry is ordinarily performed using ex-situ mixing, where the sample is mixed in an ampoule and then inserted into the calorimeter. The ex-situ mixing and thermal instability resulting from the insertion of the fresh binder into the calorimeter prevent the measurement of heat evolution during the first 30–40 min of hydration. In portland cement-based binders, this time period only involves the initial dissolution of the cement. In alkali-activated systems, significant product formation also occurs during this time period. It is therefore necessary to accurately measure the heat evolution during the very-early stages of the alkali-activation reaction. In order to do so, in-situ mixing was used in this study; the binder and activator were stored separately in a special mixing ampoule within the calorimeter until thermal stability was reached. The activator was then injected into the binder and mechanically mixed, allowing for the accurate measurement of very- early heat evolution.

3. Results

3.1. Mechanical strength

The compressive strength development of alkali-activated slag binders cured at ambient and elevated temperature is presented in Fig. 1. NaOH-activated slag develops strength rapidly at both ambient and elevated curing temperatures, as shown in Fig. 1a and b (respectively). At ambient temperature, early strength development is dependent on activator molarity. Later-age strength was independent of activator molarity. This suggests that increased activator molarity, while improving early-age strength, either has a limiting effect on later-age strength or simply results in the binder reaching it's maximum strength earlier. This is mainly due to the formation of a reaction ring on the surface of slag grains, especially with high-molarity activators [28]. The strength of NaOH-activated slag after 24 and 48 h heat curing improved with increased activator molarity, suggesting that curing at elevated temperature helps to overcome any later-age strength-limiting effects due to high-molarity activators. Most of the strength development occurred within 24 h with little improvement thereafter, as has been reported by several studies [15,21,28].

The later-age compressive strength of SS-activated slag, as shown in Fig. 1c and d, was generally higher than that of NaOH-activated slag. Despite this, the early strength development at ambient temperature was decidedly more gradual. With low sodium oxide dosages and ambient-temperature curing, specimens could only be demolded after 72 h curing due to delayed setting

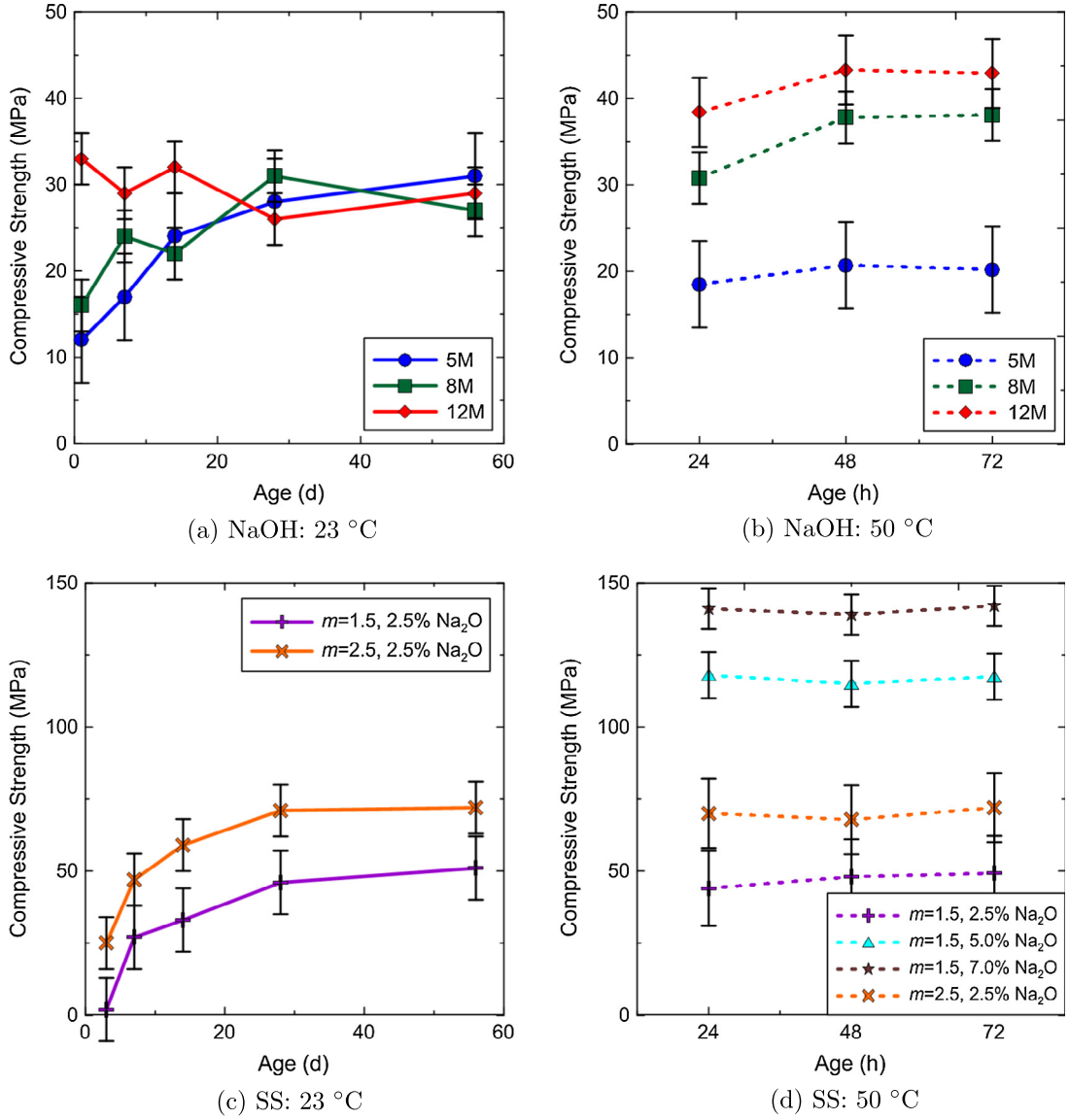

Fig. 1. Compressive strength development of alkali-activated slag binder pastes cured at ambient and elevated temperature. Note differences in scale.

and low early strength. Despite slow early strength gain in SS-activated slag, these mixtures reached equivalent strengths to NaOH-activated slag within a few days. Later-age strengths were much improved. Under ambient curing, the compressive strength improved as silica modulus increased. At elevated temperature, the strength improved as both silica modulus and sodium oxide dosage increased. Most of the strength development again occurred within 24 h. The later-age strength of specimens cured at ambient temperature was similar to the strength of those cured at elevated temperature. With very high sodium oxide dosage (7%), a strength of nearly 150 MPa was achieved.

3.2. Reaction kinetics

The reaction kinetics of the various activated slag systems studied here are presented in the following manner: The heat flow at 25 °C and 50 °C are first shown in two subfigures. Inset figures are used to magnify the very-early-age heat flow. A third subfigure simultaneously shows the cumulative heat evolution at both temperatures. The calorimetric data presented here reflect the average curve from several replicate samples, which showed little variation.

The reaction kinetics in NaOH-activated slag systems are described by Fig. 2. Two reaction peaks were identified at 25 °C, corresponding to the formation of C-S-H with various levels of aluminum, magnesium, and sodium substitution [12]. Almost no induction period was observed between these two early reaction peaks. At 12 M, the magnitude of the first peak almost completely eclipses the second. Despite drastically different heat flow during the initial dissolution, the total heat evolved after 60 h is about the same at all activator molarities. This reasonably follows the similarities in later-age compressive strength discussed in the previous section. Both are likely a result of the product formation on the surface of slag grains, which limits later-age hydration and strength gain.

The hydration of NaOH-activated slag was greatly accelerated at 50 °C. Only one major heat evolution event was recorded at all activator molarities. The most rapid parts of the reaction occurred within the first three hours, and the bulk of the heat evolution had subsided within 8 h. Increased activator molarity resulted in increased heat flow during the lone hydration event as well as increased cumulative heat flow after 60 h. This is further evidence that elevated temperatures provide the energy necessary to overcome the barriers to continued later-age hydration that are pre-

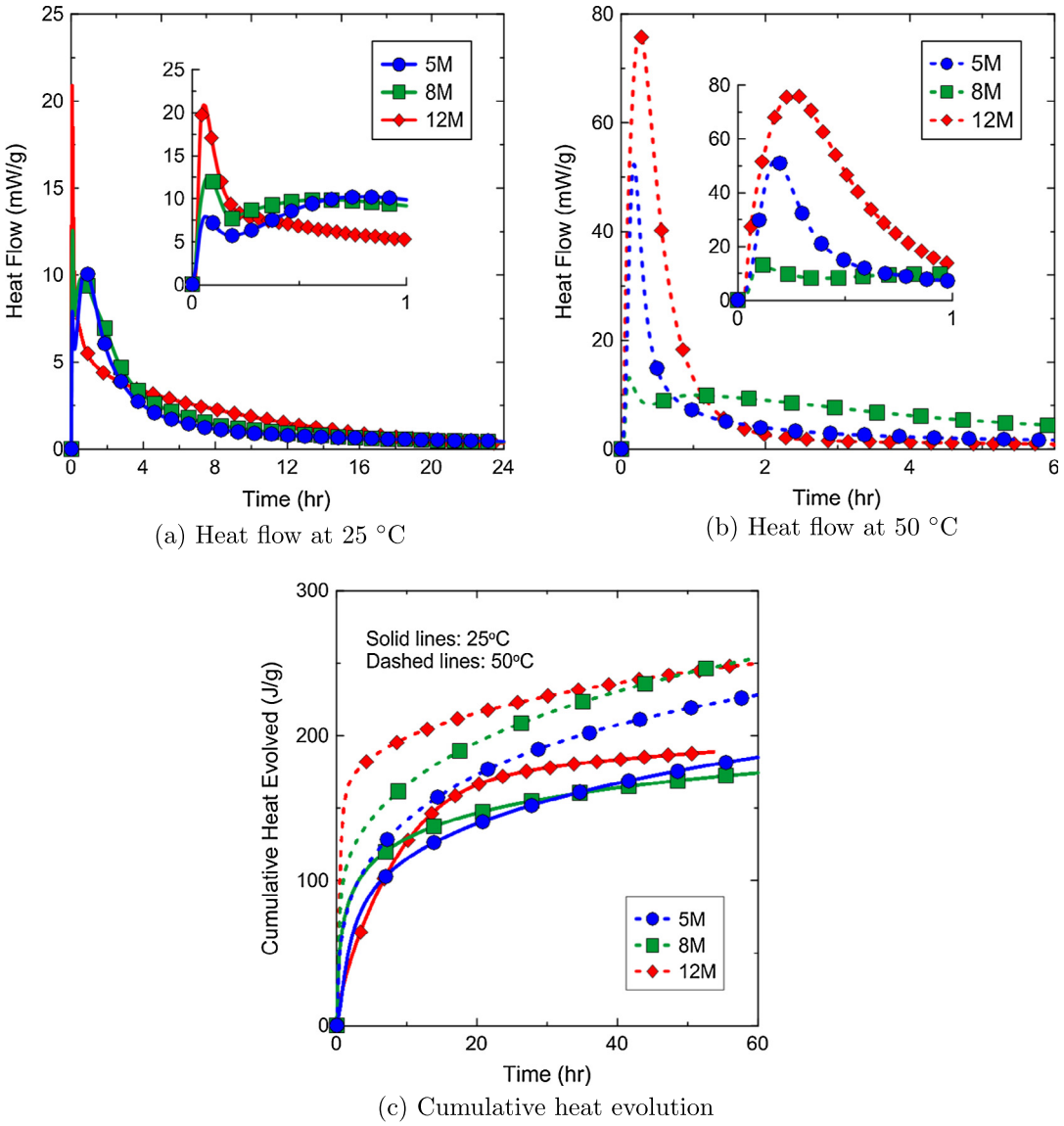

(a) Heat flow at 25 °C

(b) Heat flow at 50 °C

(c) Cumulative heat evolution

Fig. 2. Heat flow and cumulative heat evolution in sodium hydroxide-activated slag binders at varying activator molarity.

sented by high-molarity activators. The compressive strength results presented in the previous section again echo this conclusion.

The reaction kinetics in SS-activated slag systems with varying silica modulus and constant sodium oxide concentration (2.5% by mass of slag) are described by Fig. 3. At 25 °C, an early peak corresponding to initial dissolution and wetting of slag particles was followed by two additional heat evolution events. The first corresponds to early product formation, promoted by the high alkalinity of the activator solution. The second occurs as the alkalis are depleted by the early product formation and the relative silica concentration increases, promoting the dissociation of calcium [24,37]. The retarding effect of silica was indicated by the greatly delayed occurrence of the later two reaction processes, which were consequently of longer duration and lesser intensity. The bulk of the reaction processes were complete within about 72 h at 25 °C. The cumulative heat evolved was greater with lower silica modulus for the first 60 h, but thereafter identical. This is indicative of slower hydration with increased silica, but with no penalty in the degree of hydration at later age. These calorimetry data closely follow the compressive strength data for those binders cured at ambient temperature. However, the strengths at elevated temperature were improved with increased silica modulus, but the heat evolution after about 60 h is very much the same. The reason for this remains unknown.

At 50 °C, the initial dissolution of SS-activated slag was replaced by a short endothermic period lasting fewer than ten minutes. Two additional reaction peaks were again observed. The increased temperature resulted in more rapid hydration, as expected, accelerating the reaction by a factor of three or more. With lower silica modulus ($m = 1.5$), the reaction peaks occurred after about 15 min and 6 h. The increased silica at $m = 2.5$ delays the occurrence of these peaks to 2 and 9 h (respectively). The duration and intensity of both reaction events at 50 °C were affected by silica modulus in the same manner as previously discussed for 25 °C. Similarly, the cumulative heat evolved was greater with lower silica modulus for the first 12 h; thereafter, higher silica modulus resulted in greater cumulative heat evolved. This again indicates slower but more complete hydration with increased silica.

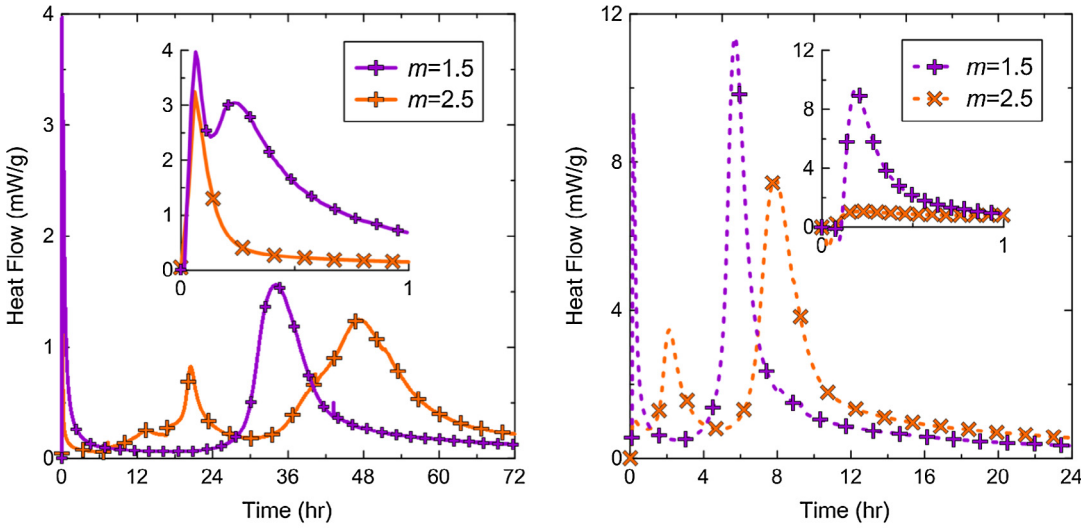

(a) Heat flow at 25 °C

(b) Heat flow at 50 °C

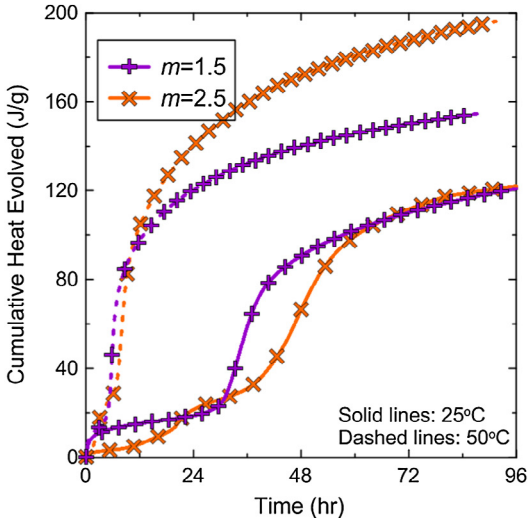

(c) Cumulative heat evolution

Fig. 3. Heat flow and cumulative heat evolution in sodium silicate-activated slag binders at varying silica modulus and constant sodium oxide concentration (2.5% by mass of slag).

The reaction kinetics in SS-activated slag with varying sodium oxide concentration and constant silica modulus ($m = 1.5$) are described by Fig. 4. At both 25 °C and 50 °C, increased sodium oxide concentration greatly accelerated hydration. This caused the dissolution and primary reaction peaks observed at low sodium oxide concentration (2.5% by mass of slag, Fig. 3)) to morph into a single high-intensity peak lasting for the first hour of the reaction. The observed effect is similar to that seen with increased activator molarity in NaOH-activated slag. The accelerating effect of increased sodium oxide at 25 °C is so great that the induction period, which lasts nearly 24 h at 2.5% Na_2O, is reduced to just one or two hours at 5% and 7% Na_2O. At 50 °C, the induction period is essentially nonexistent at 5% and 7% Na_2O. At both temperatures, the cumulative heat evolved after 60 h increased with increased sodium oxide concentration; this, combined with similar compressive strength trends, indicates more advanced hydration in SS-activated slag with higher sodium oxide dosages. As expected, the cumulative heat evolved was much greater at 50 °C than at 25 °C due to the strong accelerating effect of increased curing temperature.

3.3. Microstructure

The microstructure of NaOH-activated slag pastes with varying activator molarity is compared in Fig. 5. In backscattered scanning electron micrographs, the brightest features are the densest and the darkest are the least dense. The microstructure of such pastes has been reported to include three main phases, viz. the main reaction product (ground mass gel), incompletely-reacted slag grains, and an inner product reaction ring surrounding the unreacted slag grains [13,15,28,38]. Together, the latter two are known as the phenograins. Unreacted slag grains are visible as large white masses of the order 10 μm in diameter; these are by far the densest features of the microstructure. The inner product (reaction ring) appears as a dark gray ring surrounding the unreacted slag grains, and the ground mass gel is the lighter gray matrix that makes up the bulk of the micrograph. Although early-age micrographs are not presented, these phases were apparent after as few as six hours curing at 23 ± 2 °C. The presence of the inner product reaction ring is indicative of the diffusion-controlled reaction process where the formation of the reaction ring hinders continued diffusion [15,28].

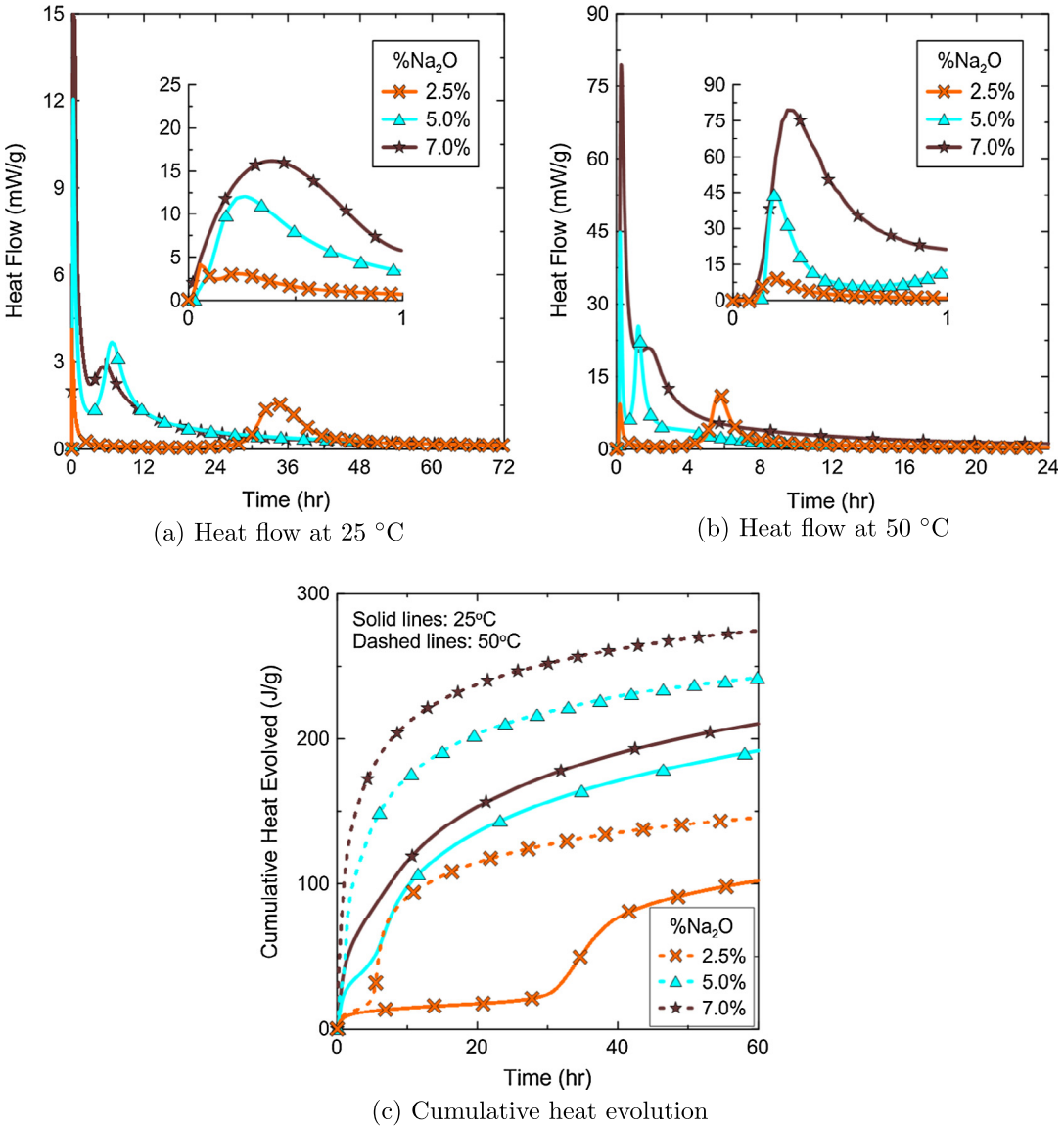

(a) Heat flow at 25 °C

(b) Heat flow at 50 °C

(c) Cumulative heat evolution

Fig. 4. Heat flow and cumulative heat evolution in sodium silicate-activated slag binders with varying sodium oxide concentration and constant silica modulus ($m = 1.5$).

Few differences were identified between the microstructure of NaOH-activated slag cured at 23 °C and 50 °C. The inner product reaction ring was observed at both curing temperatures, but the transition from ground mass gel through the inner product ring to the unreacted slag grains was more gradual at elevated temperature. The reaction rings appeared darker and more defined at ambient temperature, and were therefore likely less dense. This provides some context for the compressive strength results reported above. The diffusion-limiting effect of high-molarity activators was not observed at 50 °C, which is likely due to the formation of a denser and therefore stronger inner product at elevated temperature. In addition, more abundant nucleation sites and a reduced number of pores were visible in pastes cured at 50 °C, indicating increased product formation at elevated temperature. Some microcracking of pastes cured at elevated temperature was also observed, particularly with low-molarity activators. Since cracking generally occurs due to tensile stresses from the removal of water from the hydrated paste, and since lower-molarity activators necessarily include more abundant free water, increased prevalence of cracking at low molarity is logical.

The microstructure of SS-activated slag with varying silica modulus is compared in Fig. 6. In general, the microstructural development was slower in SS-activated slag than in NaOH-activated slag. Most of the features were not visible until about 24 h at 25 °C. Where the microstructure of NaOH-activated slag was shown to include three prominent phases, only two were observed in SS-activated slag; no prominent reaction ring was observed on the surface of the unreacted slag grains in SS-activated pastes. The lack of such a barrier to continued later-age hydration is a likely explanation for improved later-age strength development in SS-activated slag as compared to NaOH-activated slag. Both the density and homogeneity of the ground mass gel and the size of the unreacted slag grains increased with silica modulus. This indicates that, while hydration was slower with higher silica modulus, the product formed is of higher quality; the practical implication of this conclusion is that the binder will be of higher strength, as evidenced by the compressive strength values stated previously. The microstructure of pastes cured at 50 °C was more porous and visibly less refined as a result of the accelerated product formation. This suggests that the accelerated reaction results in the formation

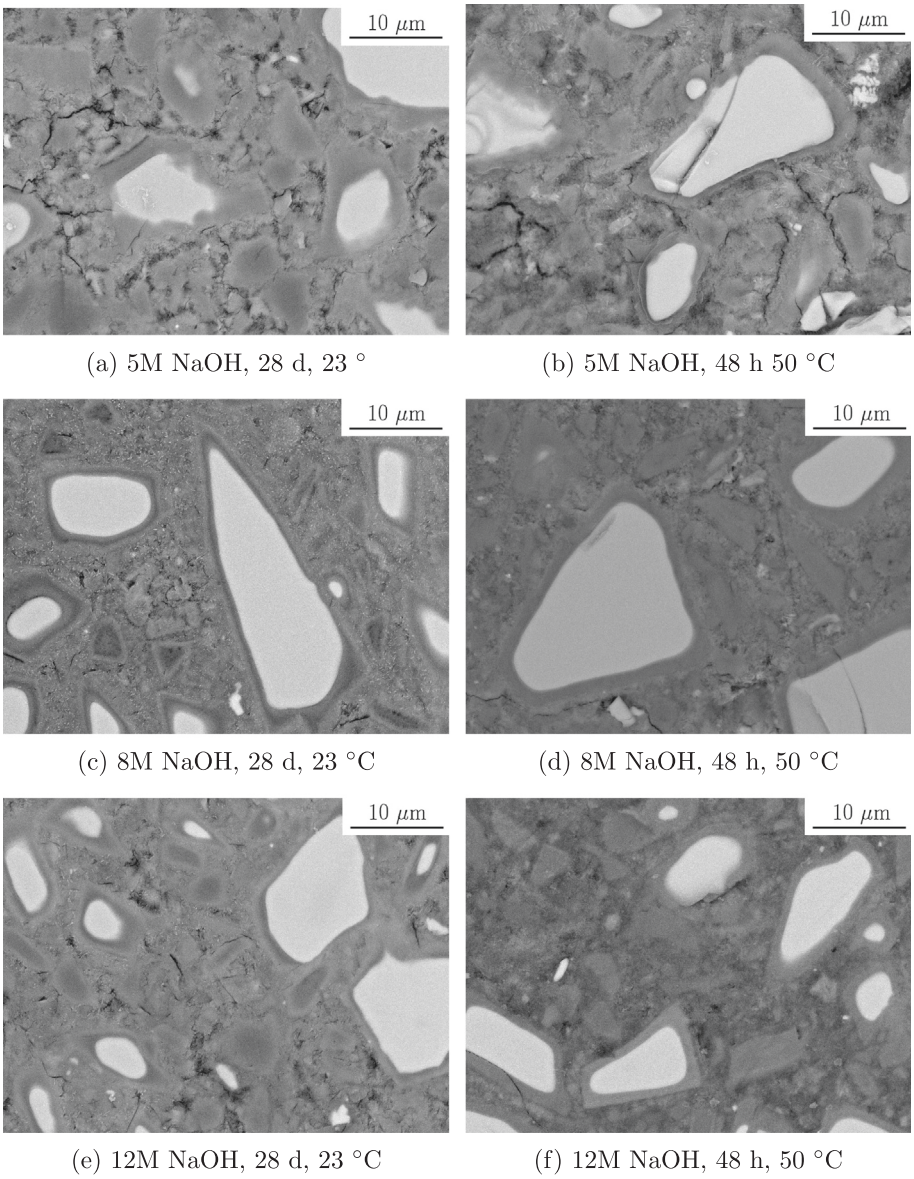

(a) 5M NaOH, 28 d, 23 °
(b) 5M NaOH, 48 h 50 °C
(c) 8M NaOH, 28 d, 23 °C
(d) 8M NaOH, 48 h, 50 °C
(e) 12M NaOH, 28 d, 23 °C
(f) 12M NaOH, 48 h, 50 °C

Fig. 5. Micrographs showing the effect of curing temperature and sodium oxide concentration on the microstructure of sodium hydroxide-activated slag binders.

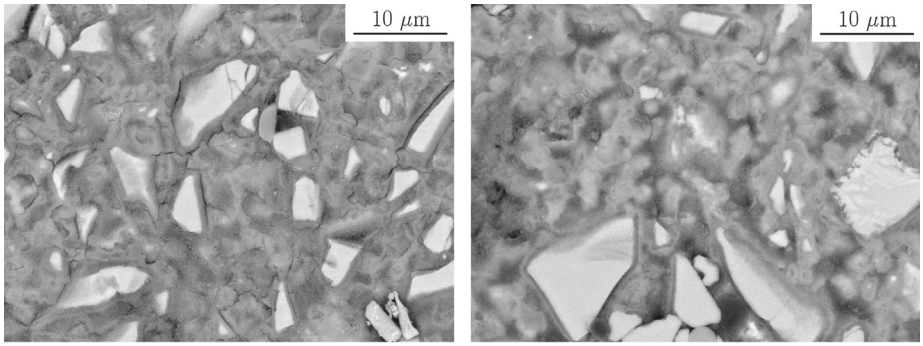

(a) $m = 1.5$, 2.5 % Na_2O, 23 °C (28 d) (b) $m = 1.5$, 2.5 % Na_2O, 50 °C (48 h)

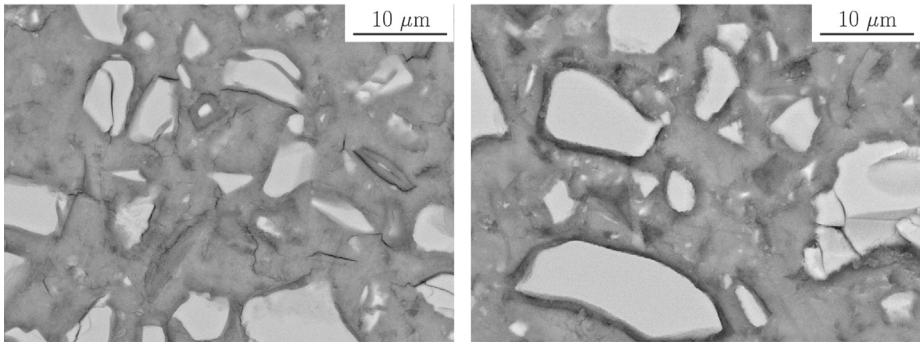

(c) $m = 2.5$, 2.5 % Na_2O, 23 °C (28 d) (d) $m = 2.5$, 2.5 % Na_2O, 50 °C (48 h)

Fig. 6. Micrographs showing the effect of curing temperature and silica modulus on the microstructure of sodium silicate-activated slag binders.

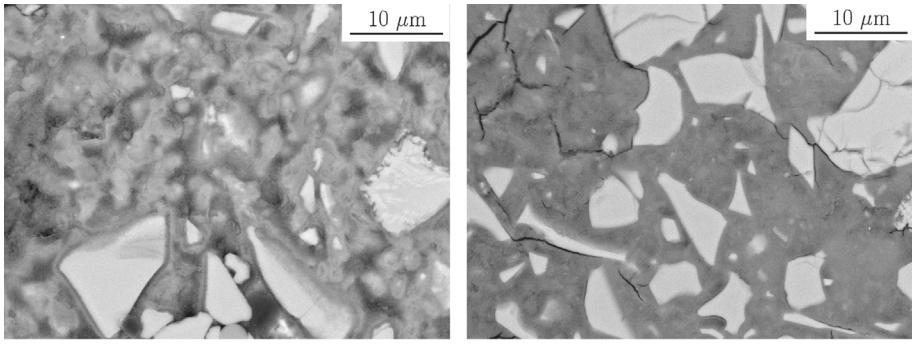

(a) $m = 1.5$, 2.5% Na_2O, 50 °C (b) $m = 1.5$, 5% Na_2O, 50 °C

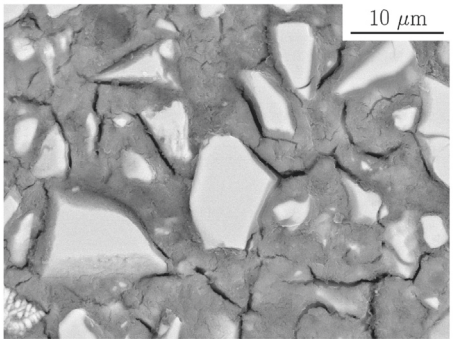

(c) $m = 1.5$, 7% Na_2O, 50 °C

Fig. 7. Micrographs showing the effect of sodium oxide concentration on the microstructure of sodium silicate-activated slag binders cured for 48 h at 50 °C.

of products of lesser density and quality. Nevertheless, the mechanical strengths were similar at both curing temperatures.

The microstructure of SS-activated slag with varying sodium oxide concentration and constant silica modulus ($m = 1.5$) is compared in Fig. 7. The density, degree of refinement, and abundance of the ground mass gel increased with sodium oxide concentration, and the physical size of the unreacted slag grains was reduced. However, the prevalence of microcracking also increased with

Table 2
Average atomic ratios for reaction products in NaOH- and SS-activated GGBFS (IP = inner product, OP = outer product).

Activator	Location	Si (atom %)		Na/Si		Mg/Si		Al/Si		Ca/Si	
		25 °C	50 °C	25 °C	50 °C	25 °C	50 °C	25 °C	50 °C	25 °C	50 °C
5 M NaOH	IP	8.3	8.9	0.15	0.14	0.35	0.42	0.38	0.27	1.36	1.21
5 M NaOH	OP	8.5	8.3	0.24	0.32	0.38	0.46	0.36	0.30	1.22	1.15
8 M NaOH	IP	8.8	9.0	0.40	0.31	0.31	0.44	0.48	0.25	1.63	1.33
8 M NaOH	OP	8.6	8.9	0.77	0.56	0.25	0.39	0.39	0.25	1.34	1.18
12 M NaOH	IP	9.2	9.6	0.51	0.79	0.24	0.31	0.36	0.21	1.81	1.41
12 M NaOH	OP	8.8	9.3	0.98	1.25	0.13	0.21	0.33	0.19	1.43	1.32
SS $m = 1.5$	OP	8.5	10.1	0.17	0.09	0.14	0.31	0.13	0.24	1.01	1.09
SS $m = 2.5$	OP	9.8	15.3	0.14	0.07	0.36	0.17	0.24	0.21	0.82	1.10

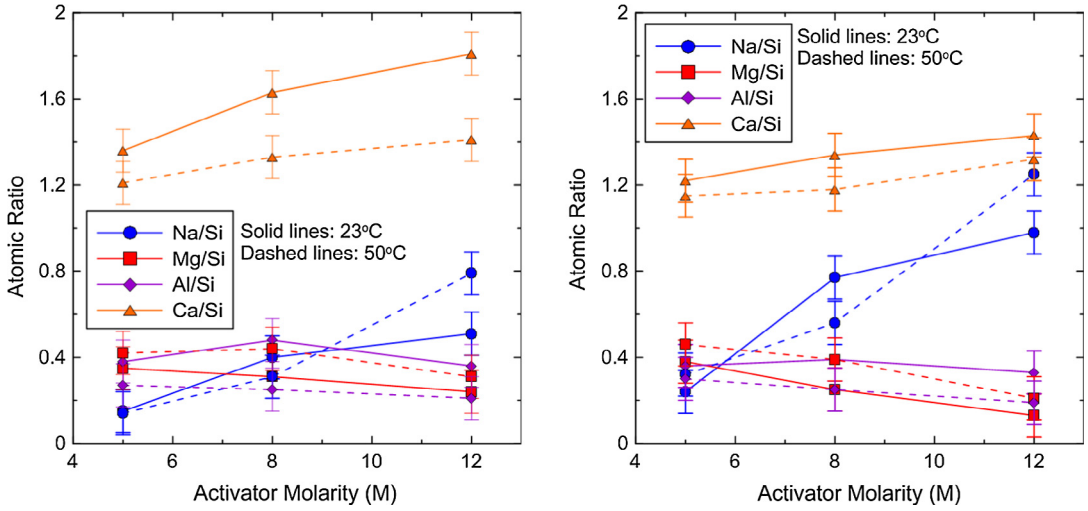

Fig. 8. Atomic ratios (Na, Mg, Al, and Ca relative to Si) in sodium hydroxide-activated slag binders cured for 28 days at 23° and 48 h at 50 °C.

sodium oxide concentration, which likely follows the enhanced brittleness of these very-high-strength pastes.

3.4. Composition

The atomic composition of alkali-activated slag binders was evaluated by EDS in conjunction with microstructural analysis using SEM. At least one dozen representative points were analyzed for each sample. The elemental compositions are presented in Table 2 and in Figs. 8 and 9. The compositions are given as the ratios of atom percentages as calculated by the EDS instrument software. The error bars in Figs. 8 and 9 represent the average atom percentage error as given by the same. The percent composition of Na, Mg, Al, and Ca are given relative to Si. For reference, the abundance of Si (in atom %) is also given in Table 2. Although it is not visible from microscopy due to the very small scale, the inclusion of large quantities of Mg and Al indicate the presence of hydrotalcite within the C-S-H product. This has been previously observed by several studies [12,31].

The abundance of Si in the inner product and ground mass gel in NaOH-activated slag increased slightly but measurably with increased activator molarity. The abundance of Si also increased slightly but measurably with curing temperature. The abundance of Na (relative to Si) in both the inner product and ground mass gel in NaOH-activated slag increased with activator molarity at both curing temperatures (Fig. 8). This of course results from the increased dosage of sodium in higher-molarity activators. There was little measurable difference in the abundance of sodium at

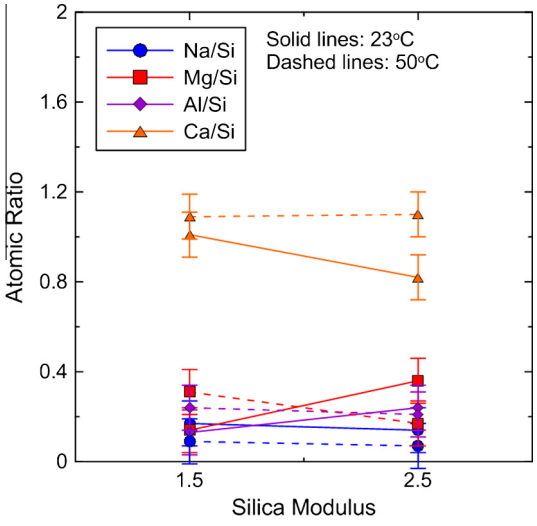

Fig. 9. Atomic ratios (Na, Mg, Al, and Ca relative to Si) in sodium silicate-activated slag binders cured for 28 days at 23° and 48 h at 50 °C.

elevated or ambient temperature. The abundance of Mg and Al (relative to Si) generally decreased as activator molarity increased, while the abundance of Ca followed the opposite trend. These changes with activator molarity were minor relative to the error of the analysis. However, the appearance of this general trend suggests the preferential formation of C-S-H with less intermixed

hydrotalcite [12,31]. This was observed at both ambient and elevated temperature, and in the inner product and ground mass gel. The effect was strongest in the inner product at ambient temperature, but only by a small margin. The abundance of Na is generally higher in the ground mass gel, while the abundance of Ca is generally higher in the inner product. The abundance of Mg and Al are about the same in the inner product and ground mass gel.

In contrast to the results presented for NaOH-activated slag, the composition of SS-activated slag (relative to Si) was essentially unchanged, at least within the margin or error of the EDS analysis. The abundance of silica increased with silica modulus, as was expected. The abundance of silica also increased with temperature, which is likely due to the increased solubility of amorphous silica from slag at elevated temperature. There was a marked decrease in the abundance of Ca (relative to Si) as the silica modulus increased at ambient temperature, but this effect was not observed at elevated temperature. This indicates that an increase in silica modulus leads to the formation of C-S-H of a lower Ca/Si ratio. The abundance of sodium was unchanged with silica modulus. This makes sense, since the dosage of sodium oxide in the activator was constant. Additionally, there was little measurable change in the abundance of Al or Mg (relative to Si).

4. Discussion

Thy hydration of sodium hydroxide-activated slag is marked by rapid product formation within thirty minutes of mixing. Increased early heat evolution at ambient temperature suggests more product formation during this period. Increase abundance of Ca and Si in the inner product suggests the formation of a denser inner product which limits later age hydration. This limits the later-age strength gain. Despite differences in early-age strength and heat evolution, the later-age strength and cumulative heat evolved are similar across molarities. Curing at elevated temperature seems to overcome this barrier to continued hydration. At 50 °C, the strength, heat evolution, and product phase composition all vary with activator molarity. The practical implication is that, while there is a limit at ambient temperature beyond which increased activator molarity will not improve mechanical strength, this can be overcome by curing at elevated temperature. Increased activator molarity tends to decrease increase the abundance of Ca and Si, and decrease the abundance of Mg and Al, suggesting that less hydrotalcite and more C-S-H is formed at higher molarities.

In stark contrast to sodium hydroxide-activated slag, the hydration of sodium silicate-activated slag is slow and controlled. Hydration is marked by the gradual formation of very dense product phases. The result is greatly improved mechanical strength which increases with both silica and sodium oxide concentration. Hydration is greatly accelerated by additions of sodium oxide and retarded by additions of silica. The reaction continues to progress through 60 h, with induction periods as long as 24 h. With high sodium oxide concentration, however, the bulk of the reaction processes may be completed within 12 h (at ambient temperature) or 4 h (at elevated temperature). The practical implication here is that both the setting time and strength of these binders may be easily tuned by adjusting the sodium oxide and silica concentration of the activator. This makes these binders extremely versatile. The increased abundance of Ca and Si at elevated temperature and with higher silica modulus suggests more complete product formation under both conditions, which is echoed by improved compressive strength.

5. Conclusions

The conclusions drawn from these information can be summarized as follows:

- In general, hydration occurs much more rapidly in sodium hydroxide-activated slag than in sodium silicate-activated slag. At ambient temperature, the microstructure of sodium hydroxide-activated slag is clearly distinguishable after as little as 6 h compared to 24 h for sodium silicate-activated slag. The heat of hydration is much lower in sodium silicate-activated slag.
- Increased activator molarity in sodium hydroxide-activated slag accelerates hydration. At ambient temperature, this rapid hydration results in the formation of an inner product reaction ring, the density of which is dependent on activator molarity. High-molarity activators, while providing excellent early strength development, limit later-age product formation due to this high-density diffusion-limiting barrier. The result of this is that the strength at ambient temperature is not improved with increased activator molarity.
- Curing sodium hydroxide-activated slag at elevated temperature greatly accelerates product formation and strength gain. Additionally, the increased temperature is sufficient to overcome the barrier to advanced hydration presented by the dense inner product ring observed with high-molarity activators. This results in improved strength with higher activator molarity when cured at elevated temperature.
- Silica in the alkaline activating solution has a distinct retarding effect on the hydration of sodium silicate-activated slag, which limits the early-age strength but results in the formation of denser product phases with higher later-age strength.
- Sodium oxide greatly accelerates hydration in sodium silicate-activated slag, resulting in significant improvements in early product formation and strength development as well as later-age strength. Very high-strength binders can be created using sodium silicate activators with high sodium oxide content.
- Elevated temperature curing greatly accelerates product formation and strength gain in sodium silicate-activated slag. These products are generally of higher density but are present at lower volume fraction within the microstructure. Additionally, elevated temperatures have a tendency to result in increasingly prevalent microcracking.

Acknowledgment

The authors gratefully acknowledge the financial support of the National Science Foundation through CMMI Award No. 1055641.

References

[1] F.S. Fulton, The Properties of Portland Cements Containing Milled Granulated Blast-furnace Slag, Portland Cement Institute, 1974.
[2] P.B. Bamforth, In situ measurement of the effect of partial portland cement replacement using either fly ash or ground granulated blast-furnace slag on the performance of mass concrete, ICE Proc, vol. 69, ICE Virtual Library, 1980.
[3] F.J. Hogan, J.W. Meusel, Evaluation for durability and strength development of a ground granulated blast furnace slag, Cem. Concr. Aggr. 3 (1) (1981).
[4] V.M. Malhotra, Fly ash, slag, silica fume, and rice-husk ash in concrete: a review, Concr. Int. 15 (4) (1993).
[5] M.D.A. Thomas, P.B. Bamforth, Modelling chloride diffusion in concrete: Effect of fly ash and slag, Cem. Concr. Res. 29 (4) (1999).
[6] V.G. Papadakis, Effect of supplementary cementing materials on concrete resistance against carbonation and chloride ingress, Cem. Concr. Res. 30 (2) (2000).
[7] ACI Committee 233, Slag Cement in Concrete and Mortar (ACI 233R-03), American Concrete Institute, 2003 (Reapproved 2011).
[8] B. Talling, J. Brandstetr, Present State and Future of Alkali-activated Slag Concretes, ACI Special Publication 114 (1989).
[9] S. Song, H.M. Jennings, Pore solution chemistry of alkali-activated ground granulated blast-furnace slag, Cem. Concr. Res. 29 (2) (1999).
[10] N.Y. Mostafa, S.A.S. El-Hemaly, E.I. Al-Wakeel, S.A. El-Korashy, P.W. Brown, Characterization and evaluation of the hydraulic activity of water-cooled slag and air-cooled slag, Cem. Concr. Res. 31 (6) (2001).

[11] S.C. Pal, A. Mukherjee, S.R. Pathak, Investigation of hydraulic activity of ground granulated blast furnace slag in concrete, Cem. Concr. Res. 33 (9) (2003).
[12] S.-D. Wang, K.L. Scrivener, Hydration products of alkali activated slag cement, Cem. Concr. Res. 25 (3) (1995).
[13] A.R. Brough, A. Atkinson, Sodium silicate-based, alkali-activated slag mortars: part i. strength, hydration and microstructure, Cem. Concr. Res. 32 (6) (2002).
[14] F. Puertas, M. Palacios, H. Manzano, J.S. Dolado, A. Rico, J. Rodŕguez, A model for the CASH gel formed in alkali-activated slag cements, J. Eur. Ceram. Soc. 31 (12) (2011).
[15] E. Deir, B.S. Gebregziabiher, S. Peethamparan, Influence of starting material on the early age hydration kinetics, microstructure and composition of binding gel in alkali activated binder systems, Cem. Concr. Compos. 48 (2014).
[16] B.C. McLellan, R.P. Williams, J. Lay, A. Van Riessen, G.D. Corder, Costs and carbon emissions for geopolymer pastes in comparison to ordinary portland cement, J. Cleaner Prod. 19 (9) (2011).
[17] L.K. Turner, F.G. Collins, Carbon dioxide equivalent (CO_2-e) emissions: a comparison between geopolymer and opc cement concrete, Constr. Build. Mater. 43 (2013).
[18] E. Douglas, J. Brandstetr, A preliminary study on the alkali activation of ground granulated blast-furnace slag, Cem. Concr. Res. 20 (5) (1990).
[19] A. Fernández-Jiménez, J.G. Palomo, F. Puertas, Alkali-activated slag mortars: mechanical strength behaviour, Cem. Concr. Res. 29 (8) (1999).
[20] F.G. Collins, J.G. Sanjayan, Workability and mechanical properties of alkali activated slag concrete, Cem. Concr. Res. 29 (3) (1999).
[21] T. Bakharev, J.G. Sanjayan, Y.-B. Cheng, Alkali activation of australian slag cements, Cem. Concr. Res. 29 (1) (1999).
[22] B. Talling, Effect of Curing Conditions on Alkali-activated Slags, ACI Special Publication 114 (1989).
[23] T. Bakharev, J.G. Sanjayan, Y.-B. Cheng, Effect of elevated temperature curing on properties of alkali-activated slag concrete, Cem. Concr. Res. 29 (10) (1999).
[24] V. Živica, Effects of type and dosage of alkaline activator and temperature on the properties of alkali-activated slag mixtures, Constr. Build. Mater. 21 (7) (2007).
[25] S. Aydn, B. Baradan, Mechanical and microstructural properties of heat cured alkali-activated slag mortars, Mater. Des. 35 (2012).
[26] E. Altan, S.T. Erdoğan, Alkali activation of a slag at ambient and elevated temperatures, Cem. Concr. Compos. 34 (2) (2012).
[27] S.A. Bernal, R. Mejía de Gutiérrez, A.L. Pedraza, J.L. Provis, E.D. Rodriguez, S. Delvasto, Effect of binder content on the performance of alkali-activated slag concretes, Cem. Concr. Res. 41 (1) (2011).
[28] B.S. Gebregziabiher, R.J. Thomas, S. Peethamparan, Very early-age reaction kinetics and microstructural development in alkali-activated slag, Cem. Concr. Compos. 55 (2015).
[29] S.-D. Wang, K.L. Scrivener, P.L. Pratt, Factors affecting the strength of alkali-activated slag, Cem. Concr. Res. 24 (6) (1994).
[30] D.M. Roy, Alkali-activated cements opportunities and challenges, Cem. Concr. Res. 29 (2) (1999).
[31] S.D. Wang, K.L. Scrivener, 29si and 27al {NMR} study of alkali-activated slag, Cem. Concr. Res. 33 (5) (2003) 769–774.
[32] Z. Huanhai, W. Xuequan, X. Zhongzi, T. Mingshu, Kinetic study on hydration of alkali-activated slag, Cem. Concr. Res. 23 (6) (1993).
[33] A. Fernández-Jiménez, F. Puertas, Alkali-activated slag cements: kinetic studies, Cem. Concr. Res. 27 (3) (1997).
[34] A. Gruskovnjak, B. Lothenbach, L. Holzer, R. Figi, F. Winnefeld, Hydration of alkali-activated slag: comparison with ordinary portland cement, Adv. Cem. Res. 18 (2006).
[35] D. Krizan, B. Zivanovic, Effects of dosage and modulus of water glass on early hydration of alkali–slag cements, Cem. Concr. Res. 32 (8) (2002).
[36] M.B. Haha, G. Le Saout, F. Winnefeld, B. Lothenbach, Influence of activator type on hydration kinetics, hydrate assemblage and microstructural development of alkali activated blast-furnace slags, Cem. Concr. Res. 41 (3) (2011).
[37] D. Rothstein, J.J. Thomas, B.J. Christensen, H.M. Jennings, Solubility behavior of Ca-, S-, Al-, and Si-bearing solid phases in portland cement pore solutions as a function of hydration time, Cem. Concr. Res. 32 (10) (2002).
[38] F. Puertas, A. Fernández-Jiménez, Mineralogical and microstructural characterisation of alkali-activated fly ash/slag pastes, Cem. Concr. Compos. 25 (3) (2003).